Mapping and statistics of ferroelectric domain boundary angles and types

Joseph Desmarais, Jon F. Ihlefeld, Tassilo Heeg, Jürgen Schubert, Darrell G. Schlom, and Bryan D. Huey

Citation: Applied Physics Letters **99**, 162902 (2011); doi: 10.1063/1.3643155
View online: http://dx.doi.org/10.1063/1.3643155
View Table of Contents: http://scitation.aip.org/content/aip/journal/apl/99/16?ver=pdfcov
Published by the AIP Publishing

Mapping and statistics of ferroelectric domain boundary angles and types

Joseph Desmarais,[1] Jon F. Ihlefeld,[2] Tassilo Heeg,[3] Jürgen Schubert,[4] Darrell G. Schlom,[3,5] and Bryan D. Huey[1,a)]
[1]*University of Connecticut, Institute of Materials Science, Storrs, Connecticut 06269, USA*
[2]*Sandia National Laboratories, Albuquerque, New Mexico 87185, USA*
[3]*Department of Materials Science and Engineering, Cornell University, Ithaca, New York 14853, USA*
[4]*Peter Grünberg Institute (PGI-9) and JARAFIT, Research Centre Jülich, Jülich D52425, Germany*
[5]*Kavli Institute at Cornell for Nanoscale Science, Ithaca, New York 14853, USA*

(Received 21 July 2011; accepted 25 August 2011; published online 17 October 2011)

Ferroelectric domain orientations have been mapped using piezo-force microscopy, allowing the calculation and statistical analysis of interfacial polarization angles, the head-to-tail or head-to-head configuration, and any cross-coupling terms. Within 1 μm^2 of an epitaxial $(001)_p$-oriented $BiFeO_3$ film, there are >40 μm of linear domain boundary based on over 500 interfaces. 71° domain walls dominate the interfacial polarization angles, with a 2:1 preference for uncharged head-to-tail versus charged head-to-head boundary types. This mapping technique offers a unique perspective on domain boundary distributions, important for ferroelectric and multiferroic applications where domain wall parameters are critical. © *2011 American Institute of Physics*. [doi:10.1063/1.3643155]

Ferroelectric domain engineering is important for its potential to improve device performance, reliability, and energy efficiency. For example, ferroelastic coupling is necessary for realizing functional multiferroic responses with $BiFeO_3$ films, and strong performance increases have been observed by isolating specific domain assemblages and structures.[1–3] Domain boundary dependent conduction is another important topic for memory applications, strain or electro-magnetic field sensors, or energy harvesting.[4,5]

There are several important domain boundary parameters. The polarization angle between adjacent domains is significant due to the corresponding ferroelastic or ferroelectric nature of these interfaces. For $BiFeO_3$, the $\langle 111 \rangle_p$ polarization directions (where *p* denotes pseudocubic indices) allow for up to 8 polarization orientation variants, reducing to 3 possible polarization angles at domain walls (180° boundaries are purely ferroelectric in $BiFeO_3$, while 71° or 109° boundaries are ferroelastic and ferroelectric). 4 possible domain boundary types or configurations are possible depending on the polarization direction of adjacent domains, where head-to-head or tail-to-tail interfaces experience opposing electric fields and are, therefore, charged, while head-to-tail or tail-to-head domains should be charge-neutral.

X-ray diffraction, electron microscopy, and piezo-force microscopy (PFM) are widely employed to investigate such ferroelectric domains and domain walls. Mapping domain orientations requires more involved measurements, however, for instance with "angle resolved" or "vector" PFM.[6–11] While such data can in principle provide maps on domain boundary angles and/or types, this is seldom performed except for a handful of domains where individual assessments have been made. This neglects the opportunity to investigate domain wall statistics and cross-correlations. Accordingly, this work presents methods for the measurement and analysis of populations of individual domain wall orientations, types, and cross-coupling.

Domain boundaries are investigated in an epitaxial, 50 nm thick, $BiFeO_3$ film, grown on a single-crystal $SrTiO_3$ substrate oriented within ±0.5° of (001) via reactive adsorption controlled molecular beam epitaxy as described elsewhere.[12,13] Briefly, an 8:1 bismuth:iron flux ratio in a 1×10^{-6} Torr oxygen/ozone (~10% ozone) background pressure and a growth temperature of 360°C was used. The film was phase-pure by x-ray diffraction and possessed a 48 arc-second omega rocking curve full-width-at-half-maximum of the 002-pseudocubic reflection, identical to the underlying substrate and indicative of high crystalline quality. Rutherford backscattering spectroscopy was used to verify film stoichiometry and revealed a bismuth:iron ratio of 1.0 (±4%):1.0 and a minimum channeling yield of 20%.

PFM was performed using an Asylum Research MFP-3d atomic force microscope (AFM) operating in contact mode

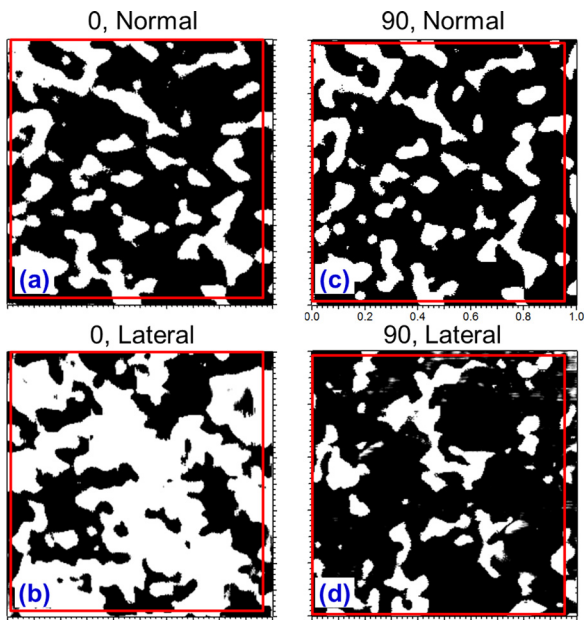

FIG. 1. (Color online) 1 μm × 1 μm PFM images of an 8-variant $BiFeO_3$ specimen with signals based on piezo-actuation in the (a) normal (z), (b) lateral (y), (c) redundantly normal (z), and (d) remaining lateral (x) directions.

a)Author to whom correspondence should be addressed. Electronic mail: bhuey@ims.uconn.edu.

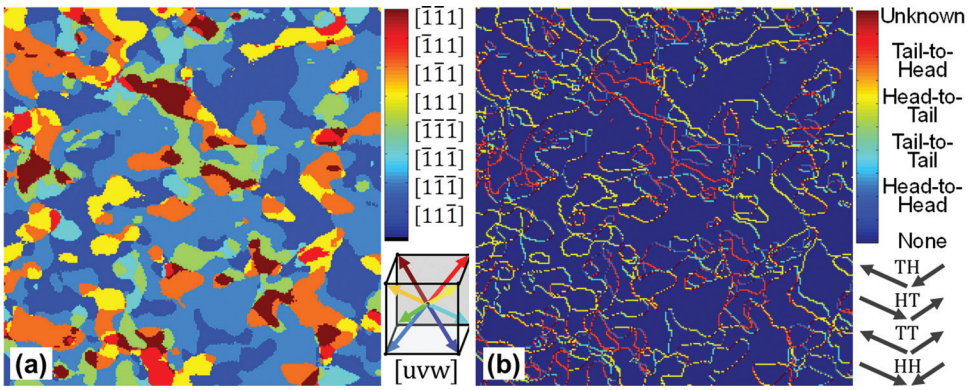

FIG. 2. (Color) Based on Fig. 1, maps are calculated of (a) domain orientation and (b) domain boundary type (head to head, tail to tail, head to tail, and tail to head).

with a conductive probe (NT-MDT DCP11).[14,15] An external function generator (Agilent 33250a) biased the probe with an AC voltage near the contact resonance, causing piezo-actuation beneath the AFM tip that was quantified with a lock-in amplifier (SRS844). Angle-resolved or vector piezo-response microscopy was employed by imaging normal (z) and lateral (x or y) signals. The distinct signals could be spectrally separated, and excited and detected simultaneously. Custom image analysis (MATLAB) was then performed to generate maps of domain boundary angles and types.

First, to determine which of the 8 possible polarization directions are present for any given region, several signals were acquired including the amplitude and phase of the piezo-response signal normal to the specimen (z) and the in-plane (lateral) response perpendicular to the cantilever long axis (y). The specimen was aligned along the $SrTiO_3$ substrate [100] axis to simplify orientation identification, though any alignment could be employed in principle. The specimen was then rotated by 90°, the same region located, and another pair of PFM images obtained for lateral and normal orientations, providing the remaining (x) direction signal and redundant normal (z) data, respectively. The 4 resulting PFM phase images identify domain orientation components along the specified directions according to dark or light contrast as shown in Fig. 1. Note that the 0° images are rotated by −90° and cropped where indicated in further analyses so that the features match based on the redundant normal piezo-response images (Figs. 1(a) and 1(c)).

Domains are identified as being polarized either into the specimen surface $[uv\bar{1}]$, or out of the sample $[uv\bar{1}]$, depending on dark or light normal PFM phase contrast, respectively. To determine which of the 4 remaining variants was present for each image pixel, the in-plane (lateral) PFM data was considered. Pixel contrast from Fig. 1(b) indicates whether variants $[u\bar{1}w]$ or $[u\bar{1}w]$ are present, while Fig. 1(d) reveals whether the domain includes components along $[\bar{1}vw]$ or $[\bar{1}vw]$. The resulting three dimensional domain orientation map is shown in Fig. 2(a), with 8 contrast levels for each of the possible polarization directions.

TABLE I. Polarization angle at domain walls, determined by matching the domain orientation on one side of a boundary (left column) with the adjacent domain's orientation (along each row).

Polarization direction	Orientation convention	71° domain boundaries	109° domain boundaries	180°
$[\bar{1}\bar{1}1]$	p_3^+	p_1^- p_4^+ p_2^+	p_2^- p_4^- p_1^+	p_3^-
$[\bar{1}11]$	p_2^+	p_4^- p_1^+ p_3^+	p_3^- p_1^- p_4^+	p_2^-
$[1\bar{1}1]$	p_4^+	p_2^- p_1^+ p_3^+	p_3^- p_1^- p_2^+	p_4^-
$[111]$	p_1^+	p_3^- p_4^+ p_2^+	p_2^- p_4^- p_3^+	p_1^-
$[\bar{1}\bar{1}\bar{1}]$	p_1^-	p_2^- p_4^- p_3^+	p_3^- p_4^+ p_2^+	p_1^+
$[\bar{1}1\bar{1}]$	p_4^-	p_3^- p_1^- p_2^+	p_2^- p_1^+ p_3^+	p_4^+
$[1\bar{1}\bar{1}]$	p_2^-	p_3^- p_1^- p_4^+	p_4^- p_1^+ p_3^+	p_2^+
$[11\bar{1}]$	p_3^-	p_2^- p_4^- p_1^+	p_1^- p_4^+ p_2^+	p_3^+

With the domain orientations mapped, domain boundaries were located by identifying positions where the domain orientation is different for adjacent pixels. Two possibilities were considered: (1) where vertically adjacent pixels were differently oriented (i.e., at a horizontal domain boundary); and (2) where horizontally adjacent domains were different (a vertical boundary). If both occurred but did not exhibit the same orientation (due to either experimental error/noise, or the site of a triple junction), the pixel was labeled as unknown and not counted for further statistical analyses. For the 1 μm^2 region imaged, 11 509 pixels were along domain boundaries, representing nearly 45 μm of linear domain wall.

A lookup table (Table I) sufficed to determine the polarization angle at each known domain wall location, based on the orientation of adjacent domains identified by convention[16] according to their polarization orientation. Although 3 distinct angles are possible, 71°, 109°, or 180°, for the specimen studied here 97.4% of the identifiable domain wall pixels exhibited 71° polarization angles. The balance were 109° boundaries (2.6%), with the population of 180° domain walls in the field of view less than 0.1%. The predominance of 71° domain walls, and the lack of 180° domain walls, are both predicted based on first-principles calculations, which indicate low and high energies for these boundaries, respectively.[17]

Domain boundary types, such as head-to-head and head-to-tail polarization configurations, were also identified for every domain wall pixel, as shown in Fig. 2(b). The four possibilities were determined based on a separate lookup table (Table II). Interestingly, domain boundary types could change if the domain wall direction changes, even though the domains are the same. Neighboring [111] and $[1\bar{1}1]$ domains (equivalently P_1^+ to P_4^+) possess a charged head-to-head configuration when left and right of a vertical domain wall, but convert to an uncharged head-to-tail configuration if the boundary turns a corner and the domains are now above and below a horizontal interface. This direction dependence of interface charging does not occur if only the normal orientation flips as with [111] and $[11\bar{1}]$ (P_1^+ and P_3^-, respectively).

Automated statistical analyses of distributions of domain boundary orientations, angles, types, and even cross-correlated terms are therefore feasible. For example, Fig. 3(a)

TABLE II Domain boundary type (head to head=HH, head to tail=HT, etc.) accounting for domain wall direction (vertical or horizontal).

Polarization direction	Orientation convention	Vertical boundary: HH (odd rows) or TT (even rows)	Vertical: HT (odd rows), TH (even rows)	Horizontal boundary: HH (odd rows) or TT (even rows)	Horizontal: HT (odd rows), TH (even rows)
$[\bar{1}\bar{1}1]$	p_3^+	$p_4^- \; p_1^+ \; p_2^+ \; p_3^-$	$p_2^- \; p_1^- \; p_4^+$	$p_2^- \; p_1^+ \; p_4^+ \; p_3^-$	$p_4^- \; p_1^- \; p_2^+$
$[\bar{1}11]$	p_2^+	$p_1^- \; p_4^+ \; p_3^+ \; p_2^-$	$p_3^- \; p_4^- \; p_1^+$	$p_3^- \; p_1^+ \; p_4^+ \; p_2^-$	$p_4^- \; p_1^- \; p_3^+$
$[1\bar{1}1]$	p_4^+	$p_3^- \; p_1^+ \; p_2^+ \; p_4^-$	$p_2^- \; p_1^- \; p_3^+$	$p_1^- \; p_2^+ \; p_3^+ \; p_4^-$	$p_3^- \; p_2^- \; p_1^+$
$[111]$	p_1^+	$p_2^- \; p_4^+ \; p_3^+ \; p_1^-$	$p_3^- \; p_4^- \; p_2^+$	$p_4^- \; p_2^+ \; p_3^+ \; p_1^-$	$p_3^- \; p_2^- \; p_4^+$
$[\bar{1}\bar{1}\bar{1}]$	p_1^-	$p_3^- \; p_4^- \; p_2^+ \; p_1^+$	$p_2^- \; p_4^+ \; p_3^+$	$p_3^- \; p_2^- \; p_4^+ \; p_1^+$	$p_4^- \; p_2^+ \; p_3^+$
$[\bar{1}1\bar{1}]$	p_4^-	$p_2^- \; p_1^- \; p_3^+ \; p_4^+$	$p_3^- \; p_1^+ \; p_2^+$	$p_3^- \; p_2^- \; p_1^+ \; p_4^+$	$p_1^- \; p_2^+ \; p_3^+$
$[1\bar{1}\bar{1}]$	p_2^-	$p_3^- \; p_4^- \; p_1^+ \; p_2^+$	$p_1^- \; p_4^+ \; p_3^+$	$p_4^- \; p_1^- \; p_3^+ \; p_2^+$	$p_3^- \; p_1^+ \; p_4^+$
$[11\bar{1}]$	p_3^-	$p_2^- \; p_1^- \; p_4^+ \; p_3^+$	$p_4^- \; p_1^+ \; p_2^+$	$p_4^- \; p_1^- \; p_2^+ \; p_3^+$	$p_2^- \; p_1^+ \; p_4^+$

presents results from a histogram of the domain orientations, revealing that nearly 70% of the domains are inward polarized while 30% are outward domains. Of course non-standard orientations, as reported elsewhere for epitaxial $BiFeO_3$ films,[11] could also be considered by modifying look-up Tables I and II, providing similar results but for a wider range of orientations and domain boundary types.

Focusing on the more interesting domain walls, the ratio of uncharged to charged interfaces was almost 2:1 (head-to-tail and tail-to-head versus head-to-head and tail-to-tail), Fig. 3(b). Such a seemingly high concentration of charged boundaries should result in sites with localized Coulombic repulsion. This may be minimized through non-standard domain orientations[11] or sub-resolution microstructural defects.

Cross-coupled terms can be determined as well using this technique. For instance, domain boundary types and proportions have been uniquely identified as a function of the local polarization angle. Head-to-head vs. head-to-tail domain boundaries occur for 32% and 68% of all 71° domain boundaries, respectively, but for 72% and 28% of 109° interfaces. Since the absolute number of such 109° domain boundaries is small in this sample, further investigations are underway into this apparent preponderance of charged 109° and neutral 71° interfaces. Future measurements will investigate links between interface parameters and film composition, orientation, annealing, etc.

In summary, this work extends ferroelectric domain orientation studies in three dimensions for automated creation of maps of domain boundary angles, types, and cross-coupling between these and/or other parameters. Such insight is crucial to efforts in engineering domain architectures, for example to optimize ferroelectric domain stability, switching speeds, switching energies, photoelectric effects, transport properties, and magnetoelectric coupling.

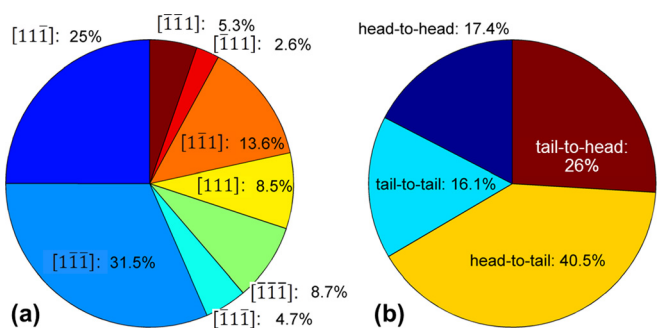

FIG. 3. (Color online) Proportions of (a) domain orientations and (b) domain wall types from Fig. 2.

BDH and JD recognize support from the Department of Energy, Grant No. DE-SC-0005037. JFI, TH, and DGS were supported by the Army Research Office, Grant No. W911NF-08-2-0032. Sandia National Laboratories is a multi-program laboratory managed and operated by Sandia Corporation, a wholly owned subsidiary of Lockheed Martin Corporation, for the U.S. Department of Energy's National Nuclear Security Administration, Contract No. DE-AC04-94AL85000.

[1]Y. H. Chu, Q. Zhan, L. W. Martin, M. P. Cruz, P. L. Yang, G. W. Pabst, F. Zavaliche, S. Y. Yang, J. X. Zhang, L. Q. Chen, D. G. Schlom, I. N. Lin, T. B. Wu, and R. Ramesh, Adv. Mater. **18**(17), 2307 (2006).
[2]H. W. Jang, D. Ortiz, S. H. Baek, C. M. Folkman, R. R. Das, P. Shafer, Y. Chen, C. T. Nelson, X. Pan, R. Ramesh, and C. B. Eom, Adv. Mater. **21**(7), 817 (2009).
[3]C. J. M. Daumont, S. Farokhipoor, A. Ferri, J. C. Wojdel, J. Iniguez, B. J. Kooi, and B. Noheda, Phys. Rev. B **81**(14), 144115 (2010).
[4]J. Seidel, L. W. Martin, Q. He, Q. Zhan, Y. H. Chu, A. Rother, M. E. Hawkridge, P. Maksymovych, P. Yu, M. Gajek, N. Balke, S. V. Kalinin, S. Gemming, F. Wang, G. Catalan, J. F. Scott, N. A. Spaldin, J. Orenstein, and R. Ramesh, Nature Mater. **8**(3), 229 (2009).
[5]A. Gruverman, D. Wu, H. Lu, Y. Wang, H. W. Jang, C. M. Folkman, M. Y. Zhuravlev, D. Felker, M. Rzchowski, C. B. Eom, and E. Y. Tsymbal, Nano Lett. **9**(10), 3539 (2009).
[6]A. Roelofs, U. Bottger, R. Waser, F. Schlaphof, S. Trogisch, and L. M. Eng, Appl. Phys. Lett. **77**(21), 3444 (2000).
[7]C. S. Ganpule, V. Nagarajan, B. K. Hill, A. L. Roytburd, E. D. Williams, R. Ramesh, S. P. Alpay, A. Roelofs, R. Waser, and L. M. Eng, J. Appl. Phys. **91**(3), 1477 (2002).
[8]F. Zavaliche, R. R. Das, D. M. Kim, C. B. Eom, S. Y. Yang, P. Shafer, and R. Ramesh, Appl. Phys. Lett. **87**(18), 182912 (2005).
[9]S. V. Kalinin, B. J. Rodriguez, S. Jesse, J. Shin, A. P. Baddorf, P. Gupta, H. Jain, D. B. Williams, and A. Gruverman, Microsc. Microanal. **12**(3), 206 (2006).
[10]R. Nath, S. Hong, J. A. Klug, A. Imre, M. J. Bedzyk, R. S. Katiyar, and O. Auciello, Appl. Phys. Lett. **96**(16), 163101 (2010).
[11]M. Park, S. Hong, J. A. Klug, M. J. Bedzyk, O. Auciello, K. No, and A. Petford-Long, Appl. Phys. Lett. **97**(11), 112907 (2010).
[12]J. F. Ihlefeld, A. Kumar, V. Gopalan, D. G. Schlom, Y. B. Chen, X. Q. Pan, T. Heeg, J. Schubert, X. Ke, P. Schiffer, J. Orenstein, L. W. Martin, Y. H. Chu, and R. Ramesh, Appl. Phys. Lett. **91**(7), 071922 (2007).
[13]J. F. Ihlefeld, N. J. Podraza, Z. K. Liu, R. C. Rai, X. Xu, T. Heeg, Y. B. Chen, J. Li, R. W. Collins, J. L. Musfeldt, X. Q. Pan, J. Schubert, R. Ramesh, and D. G. Schlom, Appl. Phys. Lett. **92**(14), 142908 (2008).
[14]R. Nath, Y. H. Chu, N. A. Polomoff, R. Ramesh, and B. D. Huey, Appl. Phys. Lett. **93**(7), 072905 (2008).
[15]N. A. Polomoff, R. N. Premnath, J. L. Bosse, and B. D. Huey, J. Mater. Sci. **44**(19), 5189 (2009).
[16]S. K. Streiffer, C. B. Parker, A. E. Romanov, M. J. Lefevre, L. Zhao, J. S. Speck, W. Pompe, C. M. Foster, and G. R. Bai, J. Appl. Phys. **83**(5), 2742 (1998).
[17]A. Lubk, S. Gemming, and N. A. Spaldin, Phys. Rev. B **80**(10), 104110 (2009).